2010

Flowfield Uncertainty Analysis for Hypersonic CFD Simulations

A B. Weaver
Purdue University

Alina A. Alexeenko
Purdue University - Main Campus, alexeenk@purdue.edu

R B. Greendyke
Air Force Institute of Technology

J A. Camberos
U. S. Air Force Research Laboratory

Follow this and additional works at: http://docs.lib.purdue.edu/aaepubs

Part of the Engineering Commons

Recommended Citation

Weaver, A B.; Alexeenko, Alina A.; Greendyke, R B.; and Camberos, J A., "Flowfield Uncertainty Analysis for Hypersonic CFD Simulations" (2010). *School of Aeronautics and Astronautics Faculty Publications.* Paper 28.
http://dx.doi.org/10.2514/6.2010-1180

48th AIAA Aerospace Sciences Meeting Including the New Horizons Forum and Aerospace Exposition
4 - 7 January 2010, Orlando, Florida

AIAA 2010-1180

Flowfield Uncertainty Analysis for Hypersonic CFD Simulations

A.B. Weaver[*] and A.A. Alexeenko[†]

Purdue University, West Lafayette, IN, 47905, United States

R.B. Greendyke[‡]

Air Force Institute of Technology, Wright-Patterson AFB, OH, 45433, United States

and J. A. Camberos[§]

U. S. Air Force Research Laboratory, Wright-Patterson AFB, OH, 45433, United States

Uncertainty quantification (UQ) in the hypersonic flow regime offers valuable information to determine physical models in need of improvement and to assist in design of vehicles and flight experiments. Here we present results of UQ analysis based on polynomial chaos method to determine flowfield and surface heat flux uncertainty under typical blunt-body re-entry conditions. The NASA Langley code, LAURA, was used for axisymmetric CFD calculations of chemically reacting hypersonic flow over FIRE-II configuration. A third order polynomial chaos (PC) method using the Gauss-Hermite quadrature was applied for determining probability density functions and moments of output quantities. Input parameters such as freestream density, velocity, and temperature were varied and the propagation of their corresponding uncertainties on output properties of interest through the flowfield were studied. An order of magnitude increase in surface heat flux uncertainties was observed for an input freestream velocity uncertainty of ±100 ft/s, or 0.29%. This parameter thus has the greatest sensitivity to variations, and conversely the freestream temperature has the least sensitivity.

Nomenclature

H_n Hermite polynomial of order n
j number of collocation points per dimension
k order of PC expansion
n order of accuracy for PC and Hermite polynomials
N number of samples
P total number of points in PC expansion
$\dot{q}$ heat flux (kW/m^2)
T translational temperature (K)
V velocity (m/s)
w weight corresponding to abscissa
x input parameter value
Y output value from solver
$\bar{Y}$ mean output value
ϵ uncertainty
ξ Gaussian random variable
μ mean
ρ density (kg/m^3)
σ standard deviation
Ψ random basis function
Subscript
i collocation point index

---

[*]Graduate Student, School of Aeronautics and Astronautics, Purdue University
[†]Assistant Professor, School of Aeronautics and Astronautics, Purdue University
[‡]Associate Professor, Dept. of Aeronautics and Astronautics, Air Force Institute of Technology
[§]Assistant to the Chief Scientist, Air Vehicles Directorate, U. S. Air Force Research Laboratory

I. Introduction

The development of advanced hypersonic aerospace vehicles remains a strong focus of several programs pursued by US Air Force and NASA[1] as well as European agencies.[2] The design of hypersonic systems requires multidisciplinary studies involving structural mechanics, aerodynamics, propulsion and materials. Since both flight and on-the-ground experiments are expensive for hypersonic flight conditions, computational methods such as computational fluid dynamics (CFD) serve as critical tools in the analysis and design of such systems. While a deterministic CFD solution gives a single-point estimate for a fixed set of input parameters, in real-life hypersonic applications numerous uncertainties in the design, manufacture and operation must be addressed. With the modern computational capabilities it has become feasible to perform uncertainty quantification (UQ) analyses which are valuable to design processes. UQ indicates which parameters are contributing the most to the variability of an output quantity and introduces opportunities for design improvements.

Stochastic UQ methods such as the Monte Carlo random sampling have been commonly used in uncertainty analysis but require typically thousands of samples and are computationally expensive. Alternate methods such as polynomial-chaos (PC) expansions use deterministic sampling. The PC method is based on the projection of the output quantity onto an orthogonal basis which can be implemented either non-intrusively at the run-level or integrated in the solver. Here we apply a non-intrusive PC approach.

There are two types of uncertainty found in CFD. One is called epistemic, which is an uncertainty originating from lack of knowledge of the true value of the metric of interest. An example would be a lack of experimental data needed to model the phenomena. The other type of uncertainty is called aleatoric, which is the uncertainty originating from random variations. For example, Champion[3] reports fluctuations in Earth atmospheric density of $\pm 5\%$ between 48 and 69 km and +4% to -16% between 70 and 80 km. The latter type of uncertainty is used in this analysis for fluctuations in atmospheric, freestream flow parameters as described next.

II. Simulation Approach and Conditions

In this study the deterministic UQ analysis is being performed for uncertainties in CFD model parameters such as chemical-kinetic rates and internal energy relaxation rates as well as atmospheric freestream flow parameters. All cases were solved using the NASA Langley code, LAURA, which is a Navier-Stokes based solver. A baseline case was considered using the forebody of the FIRE II geometry and flow conditions corresponding to the 1643 second trajectory point. The geometry of the FIRE II capsule was specified in the NASA TM X-1305[4], and is shown in figure 1 for reference (all dimensions are in cm). During the experiment there were three beryllium shields which had been ablated. The current study focuses on the peak heating rate and at which time the second beryllium shield is being utilized. Therefore the geometry specifications were taken according to the second experimental period, but only for the forebody.
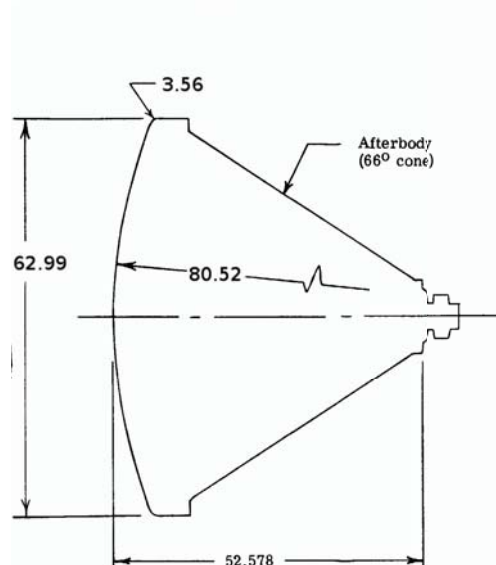

Figure 1. FIRE II Geometry

The freestream conditions including species molar concentrations based on standard atmosphere data for the given altitude are given in table 1. At these conditions significant ionization occurs and so the 11-species air model was used (N_2, O_2, NO, N, O, N^+, O^+, NO^+, e^-, N_2^+, O_2^+).

American Institute of Aeronautics and Astronautics

Table 1. FIRE II Freestream Conditions (Baseline Case)

t(s)	Altitude(km)	ρ(kg/m^3)	V(m/s)	T(K)	[N$_2$]	[O$_2$]
1643	53.04	7.8 x 10^{-4}	10,480	276	0.737795	0.262205

The boundary conditions specified on the body were: axisymmetric, constant wall temperature of 640 K, and non-catalytic. The angle of attack during reentry remained within five degrees and so axisymmetric boundary conditions were reasonable to apply. Although constant wall temperature is not realistic, it simplifies computations and in this case still agreed well with FIRE II heating data. [4] The wall was assumed to be non-catalytic for the baseline case, but is varied later. The structured grid used for the computations is shown in figure 2(a), and the final grid after adaptations and shock alignments is shown in figure 2(b).

(a) Initial Grid.

(b) Final Grid after Adaptation and Alignment.
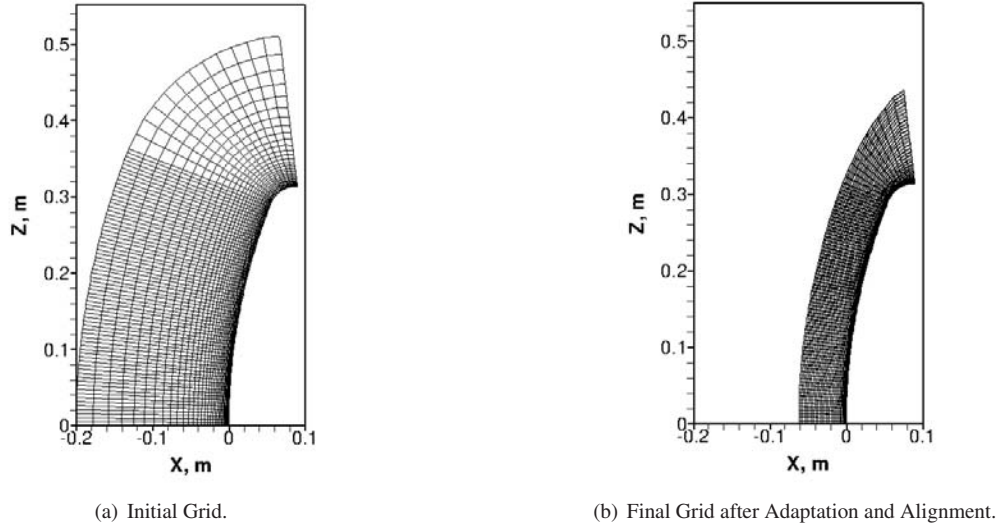
Figure 2. Structured Grid of Axisymmetric FIRE II Forebody

Input parameters were assumed to have Gaussian probability density functions (PDF) as in the analysis by Palmer [5]. Determination of the collocation points is done by first solving the zeros (abscissas) of the Hermite polynomials, which are tabulated to fifth order in table 2 [6]. By using the abscissas in an inverse form of the normal distribution the collocation points can be computed. Using the abscissas of the order of accuracy desired and the statistical parameters

Table 2. Hermite Polynomials up to Fifth Order

$$H_0(\xi) = 1$$
$$H_1(\xi) = 2\xi$$
$$H_2(\xi) = 4\xi^2 - 2$$
$$H_3(\xi) = 8\xi^3 - 12\xi$$
$$H_4(\xi) = 16\xi^4 - 48\xi^2 + 12$$
$$H_5(\xi) = 32\xi^5 - 160\xi^3 + 120\xi$$

of the input PDF, the input parameter values can be determined via Eq. (1).

$$x_i = \mu + \sqrt{2}\sigma\xi_i \tag{1}$$

where for a given input parameter, x_i is the input value corresponding to the ith abscissa, μ and σ are the mean and standard deviation of the input PDF, respectively, and ξ_i is the ith abscissa. The weights corresponding to the abscissas are determined from Eq. (2). These weights will then be used in the Polynomial Chaos expansion in order to construct

American Institute of Aeronautics and Astronautics

the output PDF as well as for the calculation of moments of output quantities within the flowfield.

$$w_i = \frac{2^{n-1}n!\sqrt{\pi}}{n^2[H_{n-1}(\xi_i)]^2} \tag{2}$$

Here, H denotes the Hermite polynomial of order (n-1), and w_i is the weight. In the PC analysis the Gauss-Hermite quadrature is utilized to calculate the moments, mean and standard deviation, of output properties. These quantities are defined in Eq. (3) - (5).

$$\bar{Y} = \frac{1}{\sqrt{\pi}} \sum_{i=1}^{P} (w_i Y_i) \tag{3}$$

$$\sigma = \sqrt{\frac{1}{\sqrt{\pi}} \sum_{i=1}^{P} w_i (Y_i(x_i) - \bar{Y})^2} \tag{4}$$

$$\epsilon = \frac{\sigma}{\bar{Y}} \tag{5}$$

The procedure to construct the output PDF of a particular flowfield property is as follows:

- First solve for the deterministic coefficients, Y_k, using the output values from the solver. The relation between the sampled output and deterministic coefficient values are given in Eq. (6).

$$\langle Y, \Psi_k \rangle = \langle \sum_{i=0}^{j} Y_i \Psi_i, \Psi_k \rangle \tag{6}$$

Due to the orthogonality of the Hermite polynomials the inner product of the random basis function is equal to zero for $j \neq k$, or $\langle \Psi_j, \Psi_k \rangle = \langle \Psi_j, \Psi_k \rangle \delta_{jk}$. Eq. (6) then becomes:

$$Y_k = \frac{\langle Y, \Psi_k \rangle}{\langle \Psi_k^2 \rangle} = \frac{1}{\langle \Psi_k^2 \rangle} \sum_{i=0}^{j} Y_i \Psi_k(\xi_i) w_i \tag{7}$$

This follows from the more general expression given by Najm[7] which applies to multi-dimensions. It is referenced here in Eq. (8)

$$Y_k = \frac{1}{\langle \Psi_k^2 \rangle} \sum_{i_1=1}^{j} \cdots \sum_{i_n=1}^{j} Y(x_{i_1}, \ldots, x_{i_n}) \Psi_k(x_{i_1}, \ldots, x_{i_n}) \prod_{k=1}^{n} w_{ik} \tag{8}$$

- Generate random samples from a normal distribution with unit variance

- Using the coefficients calculated in Eq. (8) compute the PC expansion for each random sample, j, as defined below in Eq. (9)

$$Y^j = \sum_{k=0}^{P} Y_k \Psi_k(\xi^j) \tag{9}$$

Hypersonic environments can have significant non-linearity effects between parameters and so higher dimensioned cases should be studied as well. A sparse-quadrature method can be used instead for the higher-dimensioned cases as described by Nobile et al[8].

## A.   PC Approach Verification: Fay-Riddell Stagnation Point Heating

A stagnation point heat flux analysis has been performed on a hemisphere using the Fay-Riddell correlation for varying freestream temperature and at several Mach numbers. The purpose for this particular analysis is to verify the implementation of a PC approach. A satisfactory order of accuracy in the polynomial chaos expansion will also be assessed from this.

The first and second moments are calculated for both MC and PC methods and are shown in table 3. The uncertainty in heat flux due to freestream temperature variation tends to decrease with increasing Mach number.

American Institute of Aeronautics and Astronautics

Table 3. Moments on Fay-Riddell Stagnation Point Heat Flux for Various Mach Numbers

	MC				PC					
	N = 10^6		N = 10^7		n = 2		n = 3		n = 4	
M_∞	$\mu(kW/m^2)$	$\epsilon(\%)$	$\mu(kW/m^2)$	$\epsilon(\%)$	$\mu(kW/m^2)$	$\epsilon(\%)$	$\mu(kW/m^2)$	$\epsilon(\%)$	$\mu(kW/m^2)$	$\epsilon(\%)$
3	54.20	22.074	54.20	22.085	54.20	22.076	54.20	22.091	54.20	22.091
7	894.48	17.635	894.51	17.654	894.49	17.642	894.50	17.649	894.50	17.649

A third-order PCE was used to construct the stagnation point heat flux PDF and was compared to the PDF constructed using the MC method. Both methods used one million samples and from figure 3(a) it is clear that there is good agreement. The Mach number effects on the heat flux PDF as calculated via the MC method is shown in figure 3(b). Although the standard deviation is undoubtedly larger for the higher Mach number, the mean increases at a larger rate than the standard deviation resulting in the lower level of uncertainty as already discussed.

(a) Comparison Between MC and PC Methods for $M_\infty = 3$ (b) Mach Number Effects on PDF
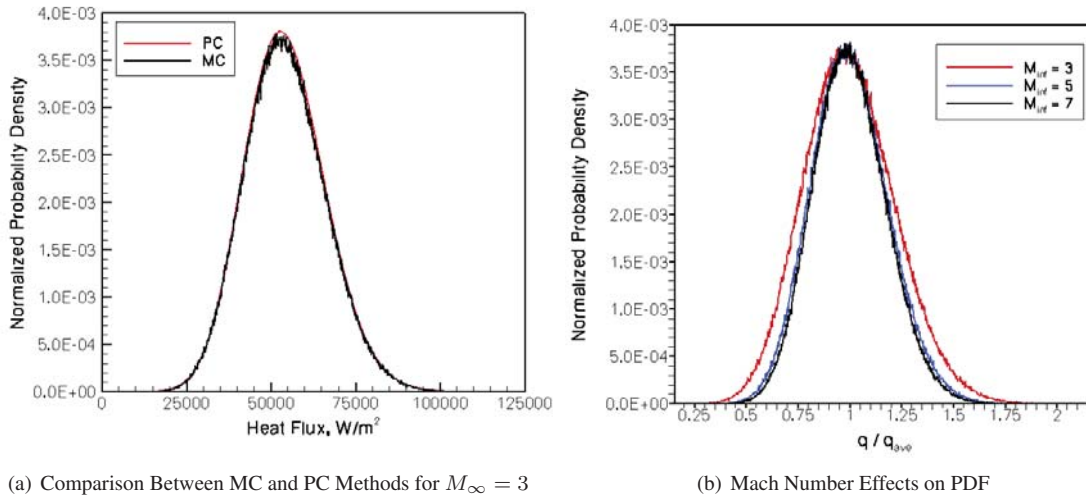
Figure 3. Fay-Riddell Stagnation Point Heat Flux

III. Results and Discussion

Here we consider effects of model uncertainties on distributed quantities such as surface heat flux and distributions of flow properties such as fields of temperature, pressure, and species concentrations. The input variance for each parameter is given in table 4. The estimated uncertainties for all parameters were taken from Palmer[5] except for the freestream velocity, which was based on uncertainty reported by Hillje[9].

Table 4. Estimated Uncertainties of Input Parameters

Parameter	Description	Uncertainty
V_∞	Freestream Velocity	$\pm$ 100 ft/s
ρ_∞	Freestream Density	$\pm$ 10%
D1,D2	Collision Integral Coefficients[10]	$\pm$ 30%
T_∞	Freestream Translational Temperature	$\pm$ 10%

A. Grid Convergence Study

A grid convergence study was performed to ensure that a sufficiently resolved grid was used. The grid was refined in the normal direction to a size of 82 streamwise x 128 normal to the body. Note for the remainder of the article the specification of grid size will always be the streamwise value followed by the normal value. At the stagnation point,

the refined grid resulted in a 0.02% higher surface heat flux. This difference increased to a maximum difference of 1.34% at a location nearly halfway around the body. Figure 4 shows the surface heat flux as a function of grid size. Following from this analysis it was determined that the 82 x 64 grid will suffice for computing the flowfield properties.
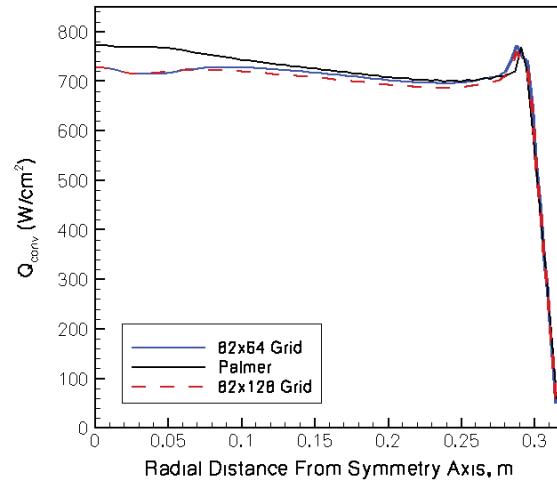

Figure 4. Grid Convergence

Figures 5(a) and 5(b) show the translational temperature and static pressure contours for the baseline case.

(a) Translational Temperature Contour
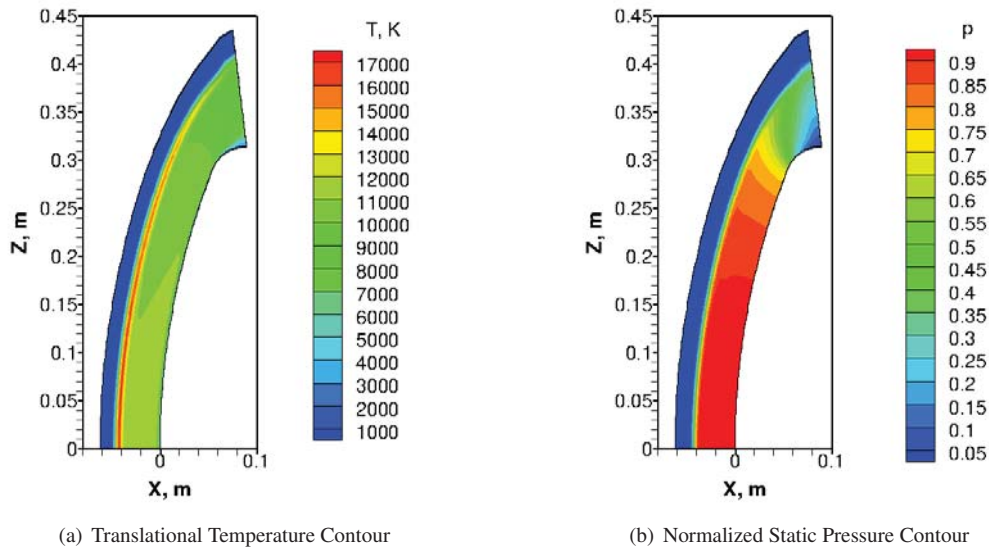
(b) Normalized Static Pressure Contour

Figure 5. Flowfield Contours for Baseline Case

B. Freestream Density Variation

Next, the effect of input uncertainty in freestream density on the surface heat flux is considered. Figures 6(a) and 6(b) show the uncertainties in translational temperature and static pressure within the flowfield, respectively. Note the regions of greatest uncertainty in temperature for an input 10% uncertainty in freestream density are: before and after the shock and in the expansion region around the shoulder.
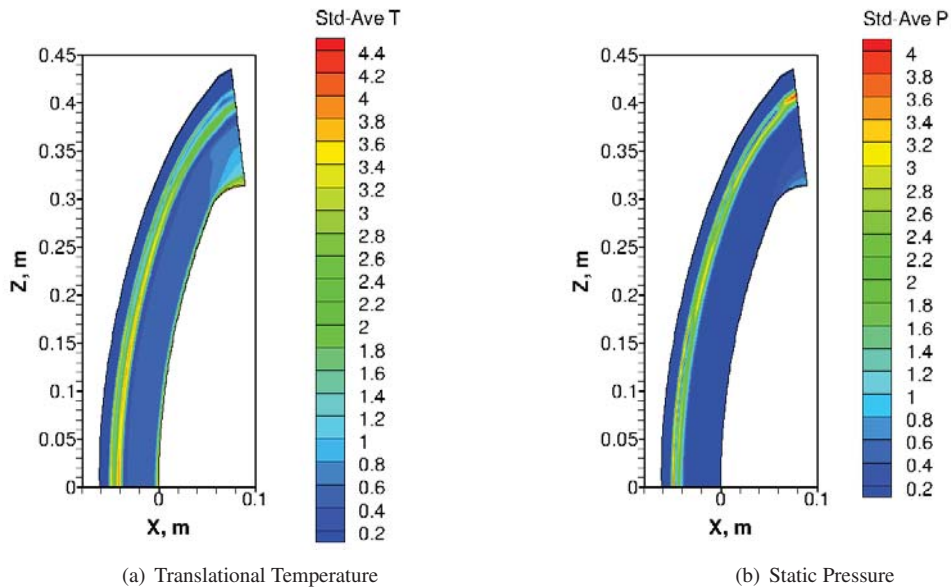
American Institute of Aeronautics and Astronautics

(a) Translational Temperature   (b) Static Pressure

Figure 6. Uncertainty Quantification in Flowfield Due to Density Variation (%)

After the shock there exists a peak in translational temperature as seen in figure 7 and hence leads to high uncertainty. This peak in the translational temperature occurs across the shock due to the initial gradients in flowfield properties across a shock and the following loss of kinetic energy to dissociate the nitrogen and oxygen molecules. Also, observe the decrease in uncertainty in the vicinity of the shock as it forms around the body.
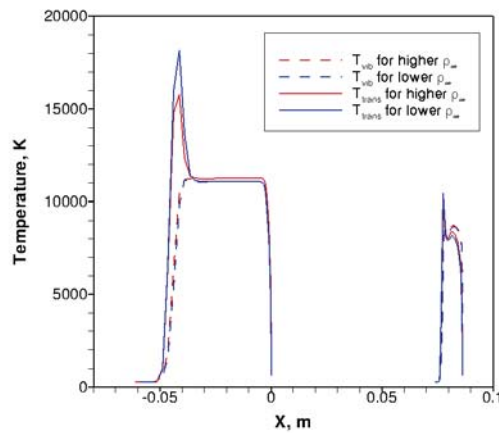

Figure 7. Translational Temperature Across Shock in Both Stagnation and Shoulder Regions

Uncertainties in the static pressures have nearly the same maximum value of 4% as for the translational temperature, however the distribution within the flowfield is different. For the static pressures, the global maximum uncertainty is located in the shoulder expansion region in the shock. Note in figure 6(b) the uncertainty is nearly the same as for translational temperature ahead of the shock, but after the shock the uncertainty is much less. The static pressure has no peak like seen for temperature, and so the maximum uncertainty is where the static pressure is least. Differences in static pressure around the shoulder region for the three freestream density cases are somewhat smaller than those seen along the stagnation streamline, but the pressures are low enough that the percent differences are greater.

A 10% variation in freestream density has a larger effect on surface heat flux with a maximum value of nearly 8.5% within the shoulder region. This is only slightly larger than at the stagnation point, which has an uncertainty of 8%. Figures 8(a) and 8(b) show the surface heat flux for the three cases and their corresponding uncertainties due to variation in freestream density, respectively.
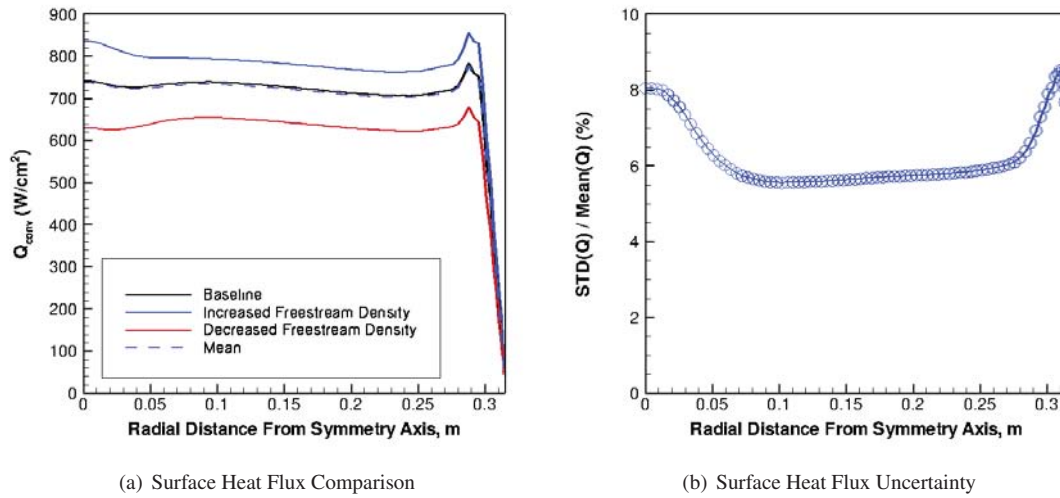
American Institute of Aeronautics and Astronautics

(a) Surface Heat Flux Comparison (b) Surface Heat Flux Uncertainty

Figure 8. Surface Heat Flux Variations Due to Density Variation (%)

The surface heat flux from the mean input density value is close to the mean of the surface heat fluxes with only slight differences between the stagnation point and shoulder regions.

C. Freestream Velocity Variation

The hypersonic flowfield is sensitive to the variation in freestream velocity. For a variation in freestream velocity of 0.29% the flowfield properties vary by more than 4.8% at their maximums. Figures 9(a) and 9(b) show the uncertainties in translational temperature and static pressure, respectively.
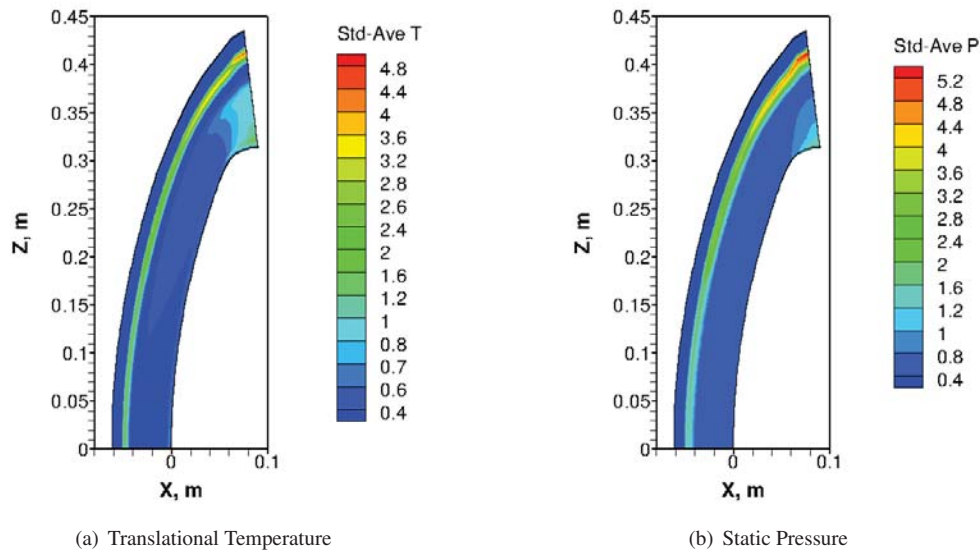

(a) Translational Temperature (b) Static Pressure

Figure 9. Uncertainty in Flowfield Due to Velocity Variation (%)

The global maximum uncertainty is located within the shock in the shoulder expansion region, and the uncertainty increases with increasing distance from the symmetry axis, Z.

Comparisons between the surface heat flux from the mean input velocity with the mean of the surface heat fluxes show more significant differences here than in the previous case with density variations. This can be seen in figure 10(a). The uncertainties in surface heat flux were also strongly affected - with an estimated input uncertainty of 0.29%, the surface heat flux uncertainty has a maximum value of 2.6%. The uncertainty in surface heat flux decreases a short distance from the stagnation point, but increases rapidly in the shoulder region to the maximum of 2.6%, as shown in figure 10(b).
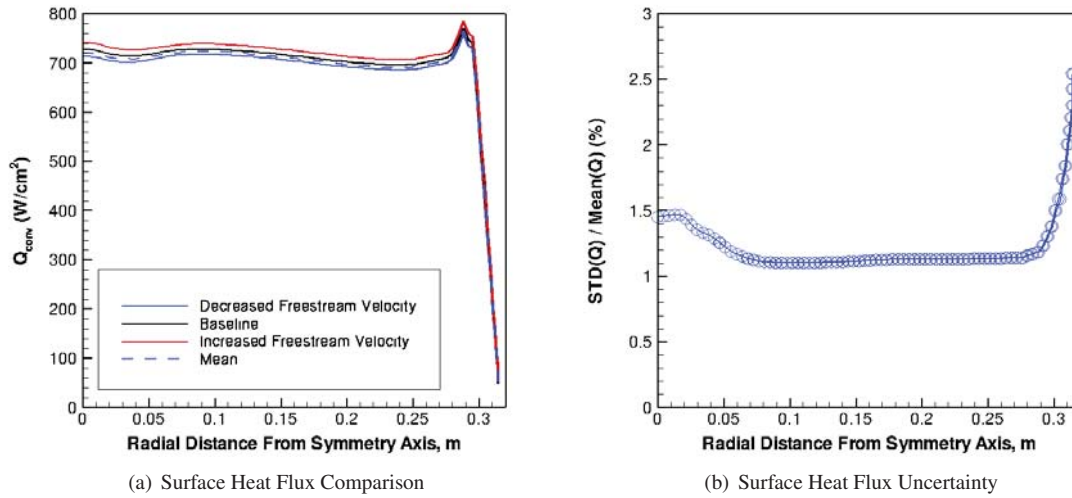
American Institute of Aeronautics and Astronautics

(a) Surface Heat Flux Comparison

(b) Surface Heat Flux Uncertainty

Figure 10. Surface Heat Flux Variations Due to Freestream Velocity Variations

Increasing freestream velocity will decrease the amount to which the flow may be turned, and adverse pressure gradients decrease the shear stress since it is a function of both the viscosity coefficient and the velocity gradient normal to the surface. It is this velocity gradient which is causing the majority of the uncertainty in the flowfield properties. At the stagnation point the velocity gradient is small, and a small variation in freestream velocity results in a larger percent difference in the velocity gradient. As the air flows around the surface the velocity gradient increases, but since this increase will be similar for each case the percent difference is less. Once the air flows around the shoulder the velocity gradient decreases, and as before the small variation in freestream velocity causes larger variation in surface heat flux.

D.   Collision Integral Coefficient Variation

Varying the collision integral coefficients effectively varies the viscosity and diffusivity of the gas species. The uncertainty in translational temperature and static pressure are shown in figures 11(a) and 11(b), respectively, for an input 30% variation in collision integral coefficients. The uncertainties are greatest within the boundary layer where the concentration of N and N_2 is also greatest. Relatively high uncertainties are found in the expansion around the shoulder as shown in figure 11(a), but this uncertainty is actually within the boundary layer and that of which particles are able to expand. A decrease in uncertainty is observable as the wall is approached.
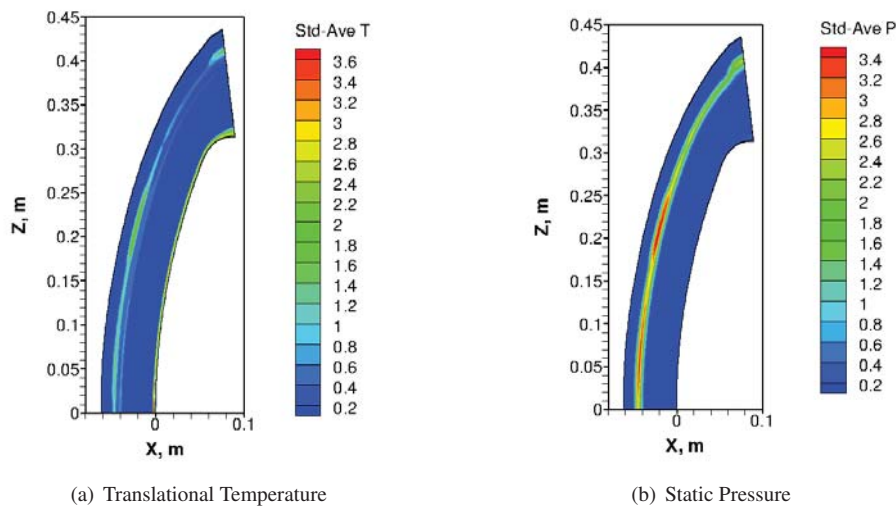

(a) Translational Temperature

(b) Static Pressure

Figure 11. Uncertainty in Flowfield Due to Collision Integral Coefficient Variation

9 of 11

American Institute of Aeronautics and Astronautics

From the 30% estimated input uncertainty the maximum uncertainty in surface heat flux was about 7.3% located in the region between the stagnation point and the shoulder. The uncertainty starts at a local minimum of 5.5% at the stagnation point and increases to the maximum value, where it remains nearly constant until the shoulder region. In the shoulder region the uncertainty decreases rapidly to a value less than 4% at the last point. As with the previous cases, the surface heat flux from the mean collision integral value was compared to the mean of the surface heat fluxes. The results show that there is very good agreement with only slight deviations between the stagnation point and shoulder regions. Figures 12(a) and 12(b) show the surface heat fluxes and their corresponding uncertainties for the variations in collision integral coefficients, respectively.
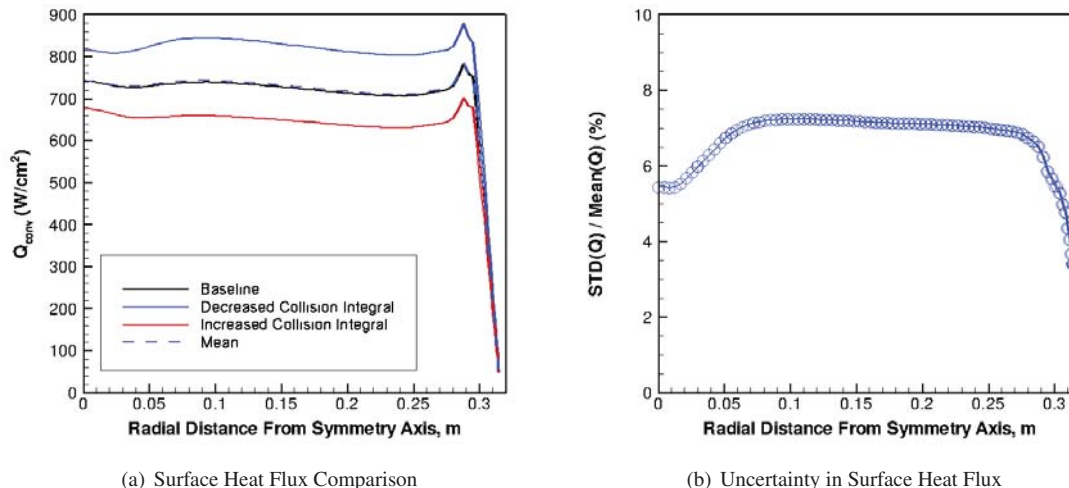
(a) Surface Heat Flux Comparison

(b) Uncertainty in Surface Heat Flux

Figure 12. Surface Heat Flux Variations Due to Collision Integral Coefficient Variations

The uncertainty drops rapidly in the shoulder region and this is due to the decrease in molecules through the expansion. Because less collisions will occur in this region, varying the collision integral will not have as much effect on heat transfer as in areas of high number densities (such as the stagnation point). As stated earlier, collision integral variations effectively varies the viscosity of the fluid, and for the stagnation point where the density is a maximum the viscosity will be most affected. Since only one collision pair out of all possible collisions is being varied, it is possible to be observing lower sensitivities to this parameter in comparison with Palmer[5] since his study had included variations for all collision pairs. It should also be noted that here an input uncertainty of 30% for the N_2-N collision integral is being used, whereas Palmer had used 30% for all collision pairs with the exception of: N_2-N, N_2-O, and N-O. Therefore, a higher dimensional scheme would need to be employed in order to test this non-linearity.

The stagnation point heating values are used to construct a PDF for varying collision integral coefficients and is shown in figure 13. The PDF is right skewed, which implies that the surface heating is more responsive to a decrease in the collision integral coefficient. The corresponding mean and standard deviation as calculated from the PDF are 733.66 and 41.18 W/cm^2, respectively.
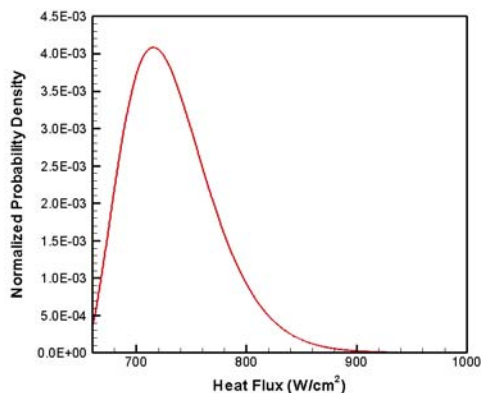
Figure 13. Surface Heat Flux PDF Due to N_2-N Collision Integral Coefficient Variation

American Institute of Aeronautics and Astronautics

IV. Conclusions

The polynomial chaos expansion (PCE) has been applied for UQ analyses of hypersonic CFD calculations for a typical blunt-body re-entry conditions. A verification of the PCE implementation is carried out by comparison with the Monte Carlo sampling for a Fay-Riddell stagnation point heat flux correlation and the third-order PCE expansion has been determined to give sufficient accuracy. The third-order PCE analysis has been applied to hypersonic flow simulations for a FIRE-II configuration. Input parameters such as freestream conditions and collision integral coefficients were varied, and their effect on the surface heating and flowfield properties were analyzed.

For freestream temperature variations, there was little effect. When freestream velocity was varied, the uncertainty in surface heating was much higher than the input uncertainty, and the maximum was located in the shoulder region where the velocity gradients at the wall are smaller. Higher translational temperature and static pressure uncertainties are likewise located in the shoulder region, but have maximums in the shock near the outflow boundary.

Varying the density had maximum uncertainties in surface heat flux both in the shoulder region and at the stagnation point. Translational temperature and static pressure had higher uncertainty levels before the shock along the stagnation streamline, but only the translational temperature also had an even higher uncertainty after the shock.

Collision integral coefficient variations had maximum uncertainty levels in surface heat flux in the region between stagnation point and the shoulder. The boundary layer had contained the highest concentration of nitrogen molecules and atoms, and therefore the maximum uncertainty in translational temperature and static pressure was located within the boundary layer.

Acknowledgments

References

[1]Ouzts, P., "The Joint Technology Office on Hypersonics," *Proc. of 15th AIAA International Space Planes and Hypersonic Systems and Technologies Conference*, 2008, also AIAA Paper 2008-2576.

[2]Falempin, F., "Possible Military Application of High-Speed Airbreathing Propulsion in the XXIst Century - an European Vision," *Proc. of AIAA International Air and Space Symposium and Exposition: The Next 100 Years*, 2003, also AIAA Paper 2003-2723.

[3]Champion, K. S. W., "Middle Atmosphere Density Data and Comparison With Models," *Adv. Space Res.*, Vol. 10, No. 6, 1990, pp. (6)17–(6)26.

[4]Cornette, E. S., "Forebody Temperatures and Calorimeter Heating Rates Measured During Project FIRE II Reentry at 11.35 Kilometers Per Second," Tech. rep., NASA Langley Research Center, Nov. 1966, also NASA TM X-1305.

[5]Palmer, G. E., "Uncertainty Analysis of CEV LEO and Lunar Return Entries," *Proc. of the 39th AIAA Thermophysics Conference*, 2007, also AIAA Paper 2007-4253.

[6]Abramotiz, M. and Stegun, I. A., *Handbook of Mathematical Functions with Formulas, Graphs, and Mathematical Tables, 9th Printing*, U.S. G.P.O., Washington, D.C., 1972.

[7]Najm, H. N., "Uncertainty Quantification and Polynomial Chaos Techniques in Computational Fluid Dynamics," *Annu. Rev. Fluid Mech.*, Vol. 41, 2009, pp. 35–52.

[8]Nobile, F., Tempone, R., and Wesbster, C., "A Sparse Grid Stochastic Collocation Method for Partial Differential Equations with Random Input Data," *SIAM J. Numerical Analysis*, Vol. 46, No. 5, 2008, pp. 2309–2345.

[9]Hillje, E., "Entry Flight Aerodynamics from Apollo Mission AS-202," Tech. rep., NASA, 1965, NASA TN D-4185.

[10]Gupta, R. N., Yos, J. M., Thompson, R. A., and Lee, K.-P., "A Review of Reaction Rates and Thermodynamic and Transport Properties for an 11-Species Air Model for Chemical and Thermal Nonequilibrium Calculations to 30,000 K," Tech. rep., NASA, 1990, NASA RP-1232.

American Institute of Aeronautics and Astronautics